Acta Cryst. (1995). D**51**, 718–724

X-ray Structure of Turkey Egg Lysozyme Complex with Di-*N*-acetyl-chitobiose. Recognition and Binding of α-Anomeric Form

BY KAZUAKI HARATA*

Biomolecules Department, National Institute of Bioscience and Human-Technology, 1-1 Higashi, Tsukuba, Ibaraki 305, Japan

AND MICHIRO MURAKI

Molecular Biology Department, National Institute of Bioscience and Human-Technology, 1-1 Higashi, Tsukuba, Ibaraki 305, Japan

(*Received* 18 *October* 1994; *accepted* 3 *January* 1995)

Abstract

The crystalline complex of turkey-egg lysozyme (TEL) with di-*N*-acetylchitobiose (NAG2) was prepared by a soaking method and the structure was determined by X-ray analysis at 1.55 Å resolution. The structure was refined to an *R* value of 0.175 by simulated annealing and energy minimization. The α-anomer of NAG2 is located at subsite *D* with the orientation perpendicular to the direction of the active-site cleft. The anomeric residue is deeply inserted into the cleft and the O1—H hydroxyl group is hydrogen bonded to the carboxyl group of Glu35 which is a catalytic residue. The other sugar residue protrudes outside the cleft and is in van der Waals contact with the β-sheet region comprising of residues 43–53. The binding of NAG2 makes the active-site cleft 0.3–0.5 Å narrower and supresses the thermal motion of two lobes constructing the cleft. The NAG2 molecule is bound in a manner not assumed in the catalytic action of the enzyme and the geometry of binding indicates that the α-anomer blocks the active center and acts only as an inhibitor.

Introduction

Lysozyme (E.C. 3.2.1.17) is an enzyme which hydrolyzes polysaccharides of bacterial cell walls. Blake *et al.* first revealed the three-dimensional structure of hen-egg lysozyme (HEL) (Blake *et al.*, 1965) and its complex with tri-*N*-acetylchitotriose (NAG3) by X-ray analysis at 2 Å resolution (Blake *et al.*, 1967). The detailed description of these structures has provided a basis for understanding the mechanism of the catalytic action of the enzyme (Imoto, Johnson, North, Phillips & Rupley, 1972; Johnson *et al.*, 1988). The active site consists of six subsites designated *A* to *F*. Six sugar residues are accommodated in the cleft and the glycosidic linkage is split between *D* and *E* subsites. To date, several crystal structures of HEL have been investigated by using high-resolution X-ray data (Rao, Hogle & Sundaralingam, 1983; Berthou, Lifchitz, Artymiuk & Jollés, 1983; Kundrot & Richards, 1987; Ramanadham, Sieker & Jensen, 1990). In the crystalline state, lysozyme binds *N*-acetylglucosamine (NAG) and its oligomers (Johnson *et al.*, 1988). The X-ray structures have revealed that the binding mode of NAG and di-*N*-acetylchitobiose (NAG2) differs according to their anomeric form (Blake *et al.*, 1967; Perkins, Johnson, Machin & Phillips, 1978; Kurachi, Sieker & Jensen, 1976). The β-anomer is bound in the active-site cleft in the manner that can be assumed in the catalytic reaction (Kurachi, Sieker & Jensen, 1976). On the other hand, Blake *et al.* (1967) have suggested that the α-anomer is bound in a different way.

Turkey-egg lysozyme (TEL) belongs to the same class of HEL and differs in seven of the 129 amino-acid residues in its primary structure (LaRue & Speck, 1970). The amino-acid sequence in the active-site region is conserved at subsites *B–F*, but the Asp101 residue located at the subsite *A* of HEL is replaced by Gly in TEL. The carboxyl group of Asp101 forms a hydrogen bond with a sugar residue of NAG3 (Blake *et al.*, 1967; Ford, Johnson, Machin, Phillips & Tjian, 1974; Strynadka & James, 1991; Cheetham, Artymiuk & Phillips, 1992). In the previous paper, we have reported the structure of a monoclinic form of TEL at 1.3 Å resolution and demonstrated that the conformation of the region of residues 100–104 differs between TEL and HEL (Harata, 1993). The structural difference in the subsite *A* may affect the binding geometry of the substrate saccharide. We have tried to obtain crystalline complexes of TEL with NAG oligomers and succeeded in the preparation of the NAG2 complex.

Materials and methods

Crystallization and data collection

Crystals of TEL were prepared according to the previously reported method (Harata, 1993). The complex with NAG2 was prepared by the soaking method. NAG2

* To whom correspondence should be addressed.

ISSN 0907-4449

was dissolved in a 10% 1-propanol solution with pH 4.2 containing 3 *M* ammonium sulfate to prepare a 5 m*M* solution. The crystals of TEL were immersed in the NAG2 solution for two weeks. Small cracks appeared at the surface of the crystals but they diffracted to the resolution of 1.5 Å. The space group was $P2_1$ and the unit-cell dimensions were $a = 38.22$, $b = 33.14$, $c = 46.00$ Å, and $\beta = 109.9°$. The crystal was isomorphous with the native crystal: $a = 38.07$, $b = 33.20$, $c = 46.12$ Å, and $\beta = 110.1°$. Intensity data were collected to 1.55 Å resolution on an Enraf–Nonius FAST diffractometer equipped with an Elliott GX21 rotating-anode generator (40 kV, 60 mA, and focal spot size 0.3 × 3 mm). Two crystals were used for the data collection. For the first crystal, 25 456 reflections were collected and were reduced to 12 834 independent reflections with the R_{merge} value of 0.107. A set of 24 543 reflections obtained for the second crystal were reduced to 11 816 independent reflections with the R_{merge} value of 0.104. These two sets of reflections were merged to produce a set of 14 142 independent reflections ($R_{merge} = 0.037$) which correspond to 88.1% of the unique reflections to the resolution of 1.55 Å.

Structure determination and refinement

The structure of the NAG2 complex of TEL was solved by the difference-Fourier method using the reflections of 10–1.55 Å resolution. The TEL coordinates determined at the 1.3 Å resolution was used as an initial model, which was refined by the simulated-annealing method using the program *X-PLOR* (Brünger, Kuriyan & Karplus, 1987). At the first stage, the model was adjusted by the energy minimization and the weight for the structure-factor term was estimated to be 59 209. In the next stage, the molecular-dynamics simulation was performed for 1 ps (1 fs step^{-1}) at 3000 K and then 0.25 ps at 300 K. Successive energy minimization for the coordinates and *B* values for individual atoms reduced the *R* value to 0.238. The difference-Fourier map clearly revealed the structure of NAG2. The atomic coordinates were estimated on the map. The NAG2 molecule was refined with the full occupancy. The energy minimization including the NAG2 molecule reduced the *R* value to 0.223. Then, water molecules were picked from Fourier and difference-Fourier maps and the refinement by the energy minimization was continued. Electron-density peaks higher than 0.3 e Å^{-3} on the $F_o - F_c$ map and having suitable intermolecular contacts were considered as water molecules, but those with the *B* value higher than 60 Å^2 were omitted. The map calculation and energy minimization were repeated three times. At each minimization stage, 40 cycles for the atomic coordinates and 20 cycles for the temperature factors were performed. At the final stage, fully occupied 80 water molecules were included in the structure model. The refinement converged at the *R* value of 0.175 for 13 430 reflections with $|F_o| > 3\sigma(F)$. The maximum values of positive and negative electron densities were 0.72 and −0.39 e Å^{-3}, respectively, and the r.m.s. residual electron density was 0.09 e Å^{-3}. No significant electron-density peaks were found in the final difference-Fourier map. The refined atomic parameters and structure factors have been deposited with the Protein Data Bank at Brookhaven.* Except for *X-PLOR*, the computer programs used were those developed in the authors' laboratory.

Results

Structure of TEL

The structure of the NAG2 complex of TEL was refined to the *R* value of 0.175 using reflections in the resolution range of 10–1.55 Å. The coordinate error (Luzzati, 1952) was estimated as 0.15–0.2 Å. The r.m.s.

* Atomic coordinates and structure factors have been deposited with the Protein Data Bank, Brookhaven National Laboratory (Reference: 1LZY, R1LZYSF). Free copies may be obtained through The Managing Editor, International Union of Crystallography, 5 Abbey Square, Chester CH1 2HU, England (Reference: AS0677).

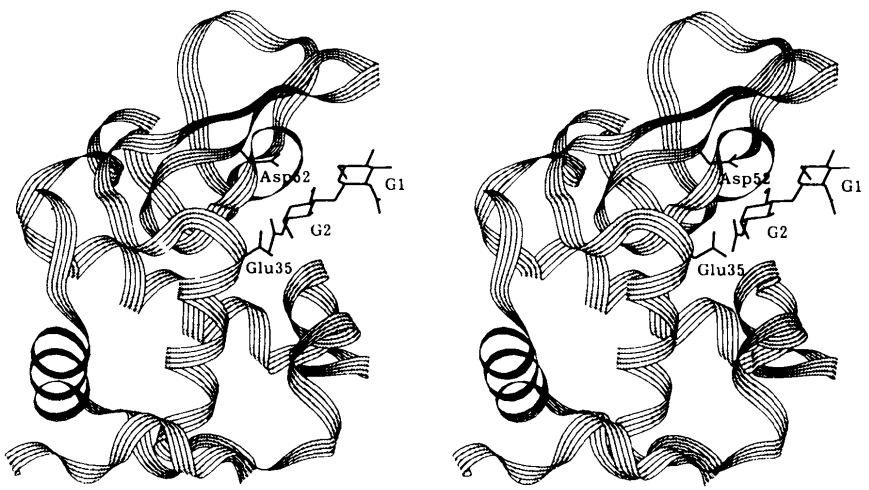

Fig. 1. A stereo drawing of the structure of TEL–NAG2 complex. The NAG2 molecule and side-chain groups of catalytically important residues, Glu35 and Asp52, are shown by thin lines.

deviations of bond distances and angles from their ideal values were 0.015 Å and 2.90°, respectively.

The structure of the NAG2 complex is shown in Fig. 1. The backbone structure of TEL is essentially the same as the structure of native TEL (Harata, 1993). The r.m.s. difference of equivalent atoms, calculated after the least-squares superposition of the TEL molecules in the native TEL and the TEL–NAG2 complex, is 0.20 Å for the C_α atoms and 0.50 Å for all protein atoms. Temperature factors averaged for main-chain peptide groups and side-chain groups are shown in Fig. 2. The average temperature factor is 13.6 $Å^2$ for all atoms, 10.6 $Å^2$ for main-chain atoms, and 16.8 $Å^2$ for side-chain atoms. Except regions of residues 47–49 and 125–129, average temperature factor of main-chain peptide groups is less than 20 $Å^2$. The positional difference of the equivalent C_α atoms between the native TEL and the NAG2 complex is plotted against the residue number (Fig. 3). The maximum difference is 0.80 Å observed at the Val109 residue. The relatively large deviation is observed in the regions of residues 40–70 and 90–120. These regions include amino-acid residues comprising the active-site cleft.

The C_α atom of Thr47 is *ca* 0.50 Å shifted from that of the native crystal. This residue is included in the turn region of Asn46–Gly49, which connects two β-strands to form a β-sheet structure. In Table 1, the φ and ψ values of these residues are compared with those of native TEL. The φ value of Asp48 becomes 20.9° smaller in magnitude by the NAG2 binding, while the ψ value changes from 11.6 to −1.1°. The relatively large change, 13.4°, is also observed in the φ value of Thr47. In the native crystal, the residues 46–49 are in a distorted β-turn classified to type I. In the NAG2 complex, the (φ, ψ) values of Thr47 and Asp48 are closer to their ideal values of the type I β-turn. The C_α atoms of Gly67 and Arg68 which are located in the loop region are moved by 0.43 and 0.49 Å, respectively, by the NAG2 binding. These residues do not participate in the formation of the active-site cleft but included in a flexible region near the cleft. The residues of Trp108, Val109 and Ala110

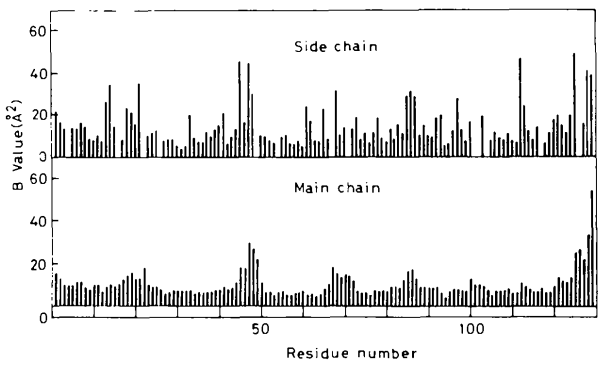

Fig. 2. Plot of average B values of main-chain and side-chain groups against the residue number.

Table 1. *Comparison of* (φ, ψ) *values* (°) *for selected residues between the NAG2 complex and native TEL*

	NAG2 complex		Native TEL	
Residue	φ	ψ	φ	ψ
Asn46	−102.4	154.5	−110.2	150.2
Thr47	−54.5	−40.0	−41.1	−40.1
Asp48	−68.3	−1.1	−89.4	11.6
Gly49	98.5	−7.6	91.0	−7.4
Asp66	−107.7	−2.2	−104.6	4.2
Gly67	89.5	−39.7	86.8	−25.8
Arg68	−84.5	−5.8	−112.7	13.4
Thr69	−110.0	111.0	−109.5	114.2
Ala107	−64.5	−15.6	−59.3	−24.6
Trp108	−99.4	108.3	−96.9	106.3
Val109	−61.7	−43.6	−71.4	−25.5
Ala110	−61.4	−37.0	−65.3	−34.0

contact with the NAG2 molecules, therefore, the structural change of this region is a result of the complex formation with NAG2. The C_α atom of Val109 is most shifted and the φ and ψ values are changed by 9.7 and 18.1°, respectively. Val109 is included in the distorted α-helix and the helix itself is slightly moved by the NAG2 binding.

As shown in Fig. 3, the temperature factors of most residues are decreased by the complex formation with NAG2. A marked decrease is observed in the regions of 40–70 and 100–120, which correspond to two lobes constructing the active-site cleft. It is noteworthy that the change in the temperature factor is correlated with the shift of C_α atoms. The prominent decrease of the temperature factor is observed for the residues showing large movement.

Structure of NAG2

The $F_o - F_c$ map calculated with the phases of TEL is shown in Fig. 4. The map was so clear that the molecular

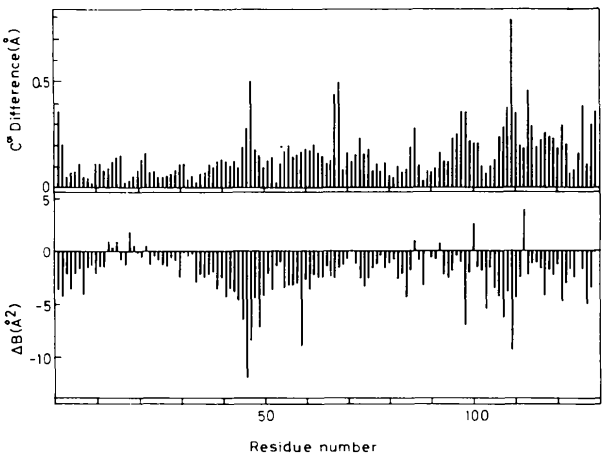

Fig. 3. Plot of positional difference of equivalent C_α atoms (upper) and B values (lower) between native TEL and the NAG2 complex. The ΔB values were calculated using averaged values for each residue as: $\Delta B = B$(NAG2 complex) − B(native TEL).

model could be constructed in the electron density. The pyranose ring of the two NAG moieties is in a normal $^4C_1$ chair conformation (Fig. 5). The average temperature factor of the molecule is 15.5 Å^2 for all atoms, 21.0 Å^2 for the G1 residue, and 10.4 Å^2 for the G2 residue. The torsion-angle index, which is defined as $\psi = |\varphi(C1—C2)| + |\varphi(C2—C3)| + |\varphi(C5—O5)| + |\varphi(O5—C1)| - |\varphi(C3—C4)| - |\varphi(C4—C5)|$, where $\varphi(C1—C2)$ is the endocyclic torsion angle O5—C1—C2—C3 of the pyranose ring, is a good estimate of the conformational change of the pyranose ring (French & Murphy, 1973). The values of the torsion-angle index for G1 and G2 are 106.9 and 115.3°, respectively, which are smaller than the corresponding values, 128.8 and 121.8°, respectively, obtained from the structure of crystalline NAG2 (Mo & Jensen, 1978). The torsion-angle index is the accumulation of small change in endocyclic torsion angles of the pyranose ring and is reflected by the change of the environment around NAG2. In both G1 and G2, the C2—N2 bond is *trans* to the C7—C8 bond. The acetyl group of the G2 residue is *ca* 35° rotated towards the O3—H hydroxyl group compared with the conformation of the corresponding acetyl group in the crystalline NAG2 (Mo & Jensen, 1978). The orientation of the C6—O6 bond is not the same between the G1 and G2 residues. The C6—O6 bond of the G1 residue is in a (−)-gauche conformation with respect to the C5—O5 bond while the (+)-gauche conformation is observed in the G2 residue. The distance, 2.9 Å, between O5 of G1 and O3 of G2 suggests the formation of O3—H···O5 hydrogen bond. This hydrogen bond imposes the restriction on the rotation of the residues around the glycosidic linkage. As a result, the values of torsion angles involving the glycosidic linkage are similar to those observed in crystalline NAG2 (Table 2).

TEL-NAG2 interaction

The NAG2 molecule is inserted into the *D* subsite of the active-site cleft. The orientation of the NAG2

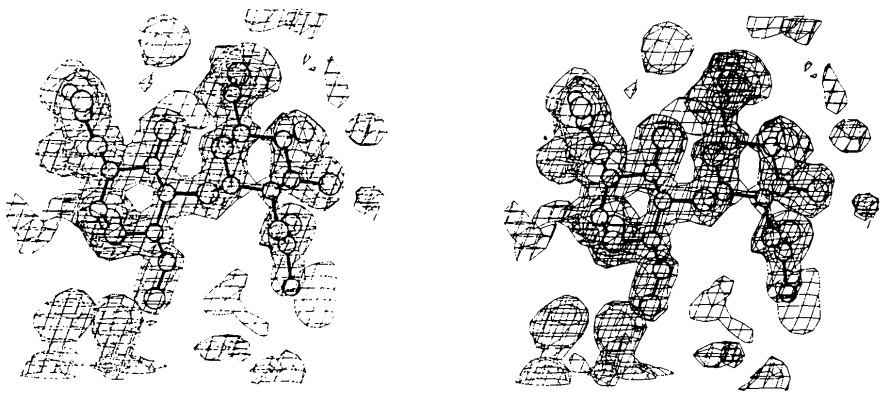

Fig. 4. The $(F_o - F_c)$ electron density for NAG2. The difference electron density was calculated after the refinement of TEL. Contours are plotted at a height of 0.2 e Å^{-3}.

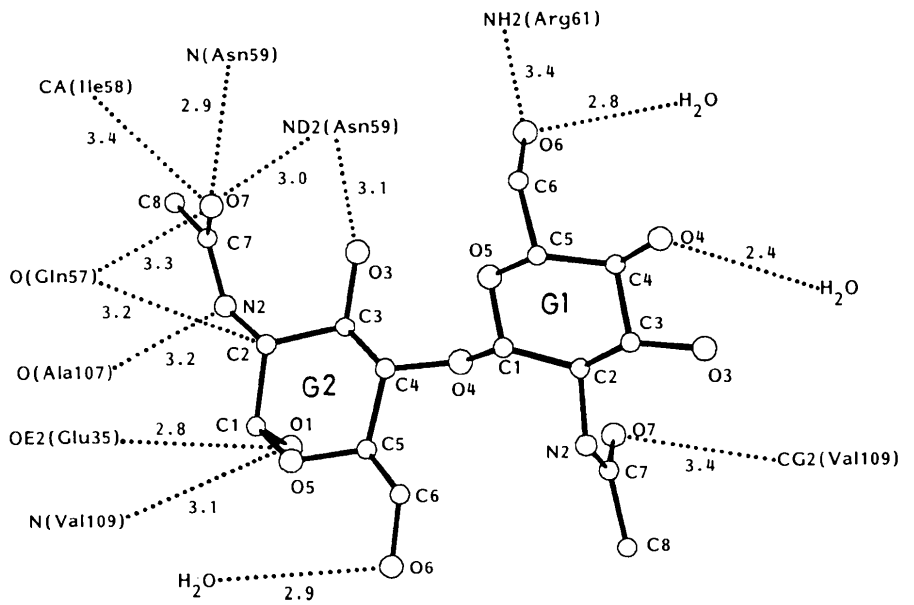

Fig. 5. Intermolecular contacts less than 3.5 Å between TEL and NAG2.

Table 2. *Torsion angles involving glycosidic linkage of NAG2*

Values in parentheses are those observed in the crystalline NAG2 (Mo & Jensen, 1978).

	Angle(°)
C2(G1)—C1(G1)—O4(G2)—C4(G2)	168.6 (161.5)
O5(G1)—C1(G1)—O4(G2)—C4(G2)	−65.9 (−79.5)
C1(G1)—O4(G2)—C4(G2)—C3(G2)	126.0 (133.5)
C1(G1)—O4(G2)—C4(G2)—C5(G2)	−114.9 (−106.8)

Table 3. *Intermolecular contacts* (Å) *between NAG2 and TEL*

Interatomic distances less than 3.8 Å are given.

	Distance (Å)		Distance (Å)
CD(Glu35)—O1(G2)	3.5	N(Asn59)—O7(G2)	2.9
OE1(Glu35)—C1(G2)	3.7	CB(Asn59)—O7(G2)	3.6
OE1(Glu35)—O1(G2)	3.7	CG(Asn59)—O7(G2)	3.6
OE2(Glu35)—C1(G2)	3.6	ND2(Asn59)—O7(G2)	3.0
OE2(Glu35)—O1(G2)	2.8	ND2(Asn59)—O3(G2)	3.0
OD1(Asn46)—O4(G1)	3.5	CD(Arg61)—O6(G1)	3.7
OD1(Asp52)—C4(G2)	3.7	NH2(Arg61)—O6(G1)	3.4
OD2(Asp52)—C6(G2)	3.7	CD1(Trp63)—O7(G2)	3.7
O(Gln57)—C1(G2)	3.2	CD(Ile98)—C8(G2)	3.6
O(Gln57)—C2(G2)	3.2	O(Ala107)—O1(G2)	3.6
O(Gln57)—N2(G2)	3.5	O(Ala107)—N2(G2)	3.2
O(Gln57)—C7(G2)	3.6	CA(Trp108)—O1(G2)	3.5
O(Gln57)—O7(G2)	3.3	NE1(Trp108)—C8(G2)	3.7
CA(Ile58)—O7(G2)	3.4	N(Val109)—O1(G2)	3.1
C(Ile58)—O7(G2)	3.6	CG2(Val109)—O7(G1)	3.4

molecule is nearly perpendicular to the direction of the cleft and parallel to the β-sheet formed of residues 43–53 (Fig. 6). The active-site structure including the NAG2 molecule is shown in Fig. 7. The G1 residue protrudes from the cleft and mostly exposed to solvent. The pyranose ring is in van der Waals contact with residues Asn46, Thr47 and Asp48. The side-chain group of Asn46 is facing the pyranose ring at a distance of *ca* 4 Å (Table 3). The primary hydroxyl group of G1 makes contacts with residues 59–62. The O4—H hydroxyl group is linked to the carboxyl group of Asp48 by a water-mediated hydrogen-bond bridge. The acetyl group points to the outside of the cleft and is in van der Waals contact with the side-chain group of Val109.

The G2 residue is deeply inserted into the active-site cleft. The acetyl group is in close contact with the main-chain carbonyl group of Gln57. The conformation of the O1—H hydroxyl group is an α-anomeric form. Since the O(Gln57) atom is close to the C1 and C2 atoms of the G2 residue (3.2 Å), the accommodation of the O1—H group with the β-anomeric form is impossible. The O1—H hydroxyl group forms hydrogen bonds with OE2(Glu35) and N(Val109) and links the ends of two α-helices by the OE2(Glu35)···O1···O(Val109) hydrogen-bond bridge. The acetyl group is surrounded by Gln57, Ile58 and Asn59. The O7 atom of the acetyl group forms hydrogen

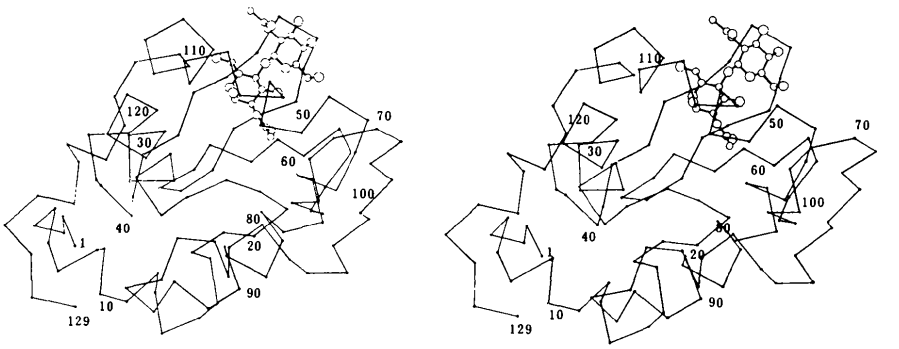

Fig. 6. A stereo drawing of the NAG2 complex of TEL. Atoms in NAG2 are shown by open circles.

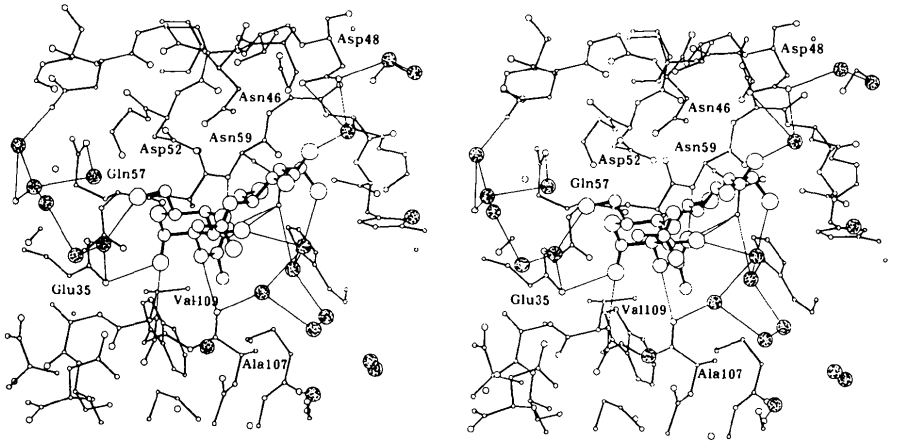

Fig. 7. A stereo drawing of the structure of the NAG2-binding site. Atoms in NAG2 are shown by open circles. Water molecules are shaded. Thin lines denote possible hydrogen-bonding contacts.

bonds with N and ND2 of Asn59. The N2 atom is hydrogen bonded to O(Ala107). These hydrogen bonds link the two regions separated by the cleft and form a bridge across the cleft. The side-chain group of Asp52 faces to the pyranose ring of the G2 residue and is in van der Waals contact with C4, C6 and O5 atoms. The primary hydroxyl group is exposed to solvent and forms a hydrogen bond with a water molecule.

Crystal packing and intermolecular contacts

The TEL molecule contacts with four molecules located parallel to the *ac* plane and two molecules along the *b* axis. The active-site cleft is open to the intermolecular space although the subsites *A*, *B* and *F* are blocked by adjacent molecules. Therefore, the NAG2 molecule can diffuse into the solvent channel running parallel to the *b* axis and is inserted into the *D* subsite of TEL. The acetyl group of the G1 residue contacts with the side-chain group of Arg125 in a symmetry-related TEL molecule. The shortest distance, 3.5 Å, is found between C8(G1) and NE(Arg125) $(1-x, -\frac{1}{2}+y, 1-z)$. A close contacts between TEL molecules are observed with the molecule related by the twofold screw axis $(1-x, \frac{1}{2}+y, 1-z)$, where the main-chain peptide groups are in a distance of 2.9 Å. Adjacent molecules are also linked by water-mediated hydrogen-bond bridges.

Discussion

The crystallographic study of the TEL complex with NAG2 shows that the NAG2 molecule with the α-anomeric residue is bound in the orientation that could not be assumed in the catalytic reaction. Many structures of HEL complexed with mono- and oligosaccharides have been investigated by X-ray analysis (Johnson *et al.*, 1988). Kurachi *et al.* have reported the HEL complex with NAG2 which has a β-anomeric residue (Kurachi, Sieker & Jensen, 1976). In that structure, the β-anomer of NAG2 is bound to the *B* and *C* subsites in the same manner found in the binding of the β-anomer of NAG3 to HEL. The difference in the binding of α- and β-anomers of NAG to HEL has been investigated by Perkins *et al.* (1978). The β-NAG molecule is accommodated at the *B* subsite of HEL in the same manner as that found in the HEL complexes with β-anomeric oligomers. In contrast, α-NAG is bound to HEL in a similar manner to that of the G2 residue of NAG2 in the TEL–NAG2 complex. Therefore, the orientation of saccharide bound in the active-site cleft differs according to the anomeric form.

It is noteworthy that the hydrogen-bond formation of the acetyl group of G2 with Asn59 and Ala107 is commonly observed in both the TEL complexes with the α-anomer of NAG2 and the HEL complex with the β-anomer. The N2 and O7 atoms of the acetyl group are hydrogen bonded to O(Ala107) and N(Asn59), respectively, and form a bridge between the polypeptide chains of both sides of the cleft. The orientation of the α-anomer of NAG2 in the TEL complex coincides with that of the β-anomer in the HEL complex when it is *ca* 90° rotated around the bridge. The acetyl group is a pivot of the transformation of the NAG2 position from one anomer to the other. The α-anomer of NAG2 seems to be more strongly bound to the cleft of TEL than the β-anomer in the HEL complex. The O1—H hydroxyl group of the β-anomer of NAG2 has no direct contact with HEL. On the other hand, the O1—H group of the α-anomer of NAG2 is hydrogen bonded to Glu35 and Val109. The α-anomer could be bound to TEL in the same manner as that of the β-anomer in the HEL complex. However, the binding mode in the present structure is more favorable with the increasing number of hydrogen bonds with the protein. Furthermore, the hydrogen-bond bridge of OE2(Glu35)—O1—N(Val109) in addition to N(Asn59)···O7—C7—N2···O(Ala107) will stabilize the protein structure by an effect similar to that caused by the cross-linking. The conformation of the side-chain group of Glu35 is not significantly affected by the hydrogen-bond formation with the α-anomer of NAG2. In contrast, the Val109 residue is moved by 0.8 Å in its C_α position and the average *B* value is decreased by 9.3 Å^2. The prominent decrease of the *B* value is also observed in Asn59 and Ala107, of which the temperature factors are lower than those of native TEL by 9.0 and 6.3 Å^2, respectively. The temperature factors of the O1—H and acetyl groups of the G2 residue are in the range from 6.8 to 9.4 Å^2. These values are of a similar magnitude to those of amino-acid residues involving the

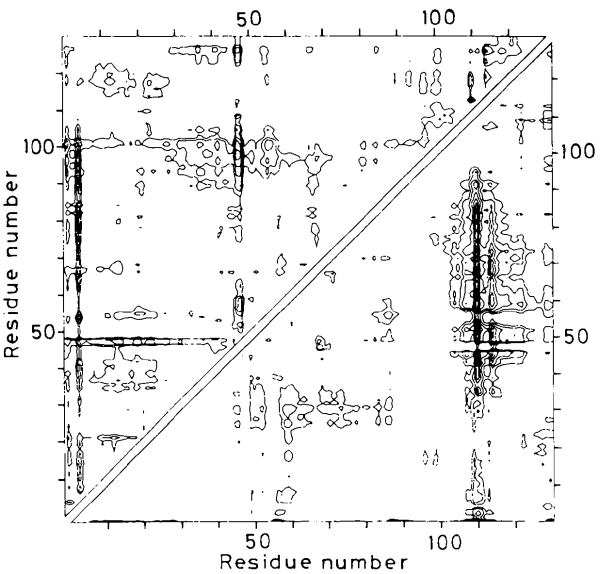

Fig. 8. Difference distance map between native TEL and the NAG2 complex. The difference of C_α–C_α distances, Δr_{ij}(NAG2 complex) − Δr_{ij}(native TEL), is plotted. Contours are drawn at 0.1, 0.2, 0.3 Å (top left) and −0.1, −0.2, −0.3 Å (bottom right).

NAG2 binding. The same tendency has been observed in the HEL complexes with trisaccharides (Ford *et al.*, 1974; Strynadka & James, 1991; Cheetham, Artymiuk & Phillips, 1992). However, the temperature factor of NAG2 is markedly lower than that of those trisaccharides in the HEL complexes. These results indicate that the binding of the α-anomer of NAG2 suppresses the thermal motion of the cleft by the bridging effect through hydrogen bonds.

The direction of the relative movement of each amino-acid residue caused by the NAG2 binding can be estimated from the difference distance map shown in Fig. 8. The distance between C_α atoms is compared with that of native TEL. The residues 3–5 are moved away from residues 5–105. The residues of 47–48 are also moved away from most of the other residues. The movement of these residues are caused by the change in the β-turn structure as indicated from the comparison of (φ, ψ) angles (Table 1). A prominent decrease in the C_α distance is observed between two regions, 30–90 and 100–120. These two regions, which are separated by the active-site cleft, become nearer by the binding of NAG2. Therefore, the active-site cleft of the NAG2 complex is narrower than the cleft of native TEL and the width of the cleft is decreased by 0.3–0.5 Å as measured between C_α atoms. The C_α atom of Val109 moves more than 0.6 Å toward residues 35–46, 49–53 and 57–86. A similar structural change induced by the binding of sugars has been observed in HEL although no quantitative estimation of the movement has been made. The binding of NAG2 imposes restrictions on the hinge-bending motion of two lobes of the active-site cleft. These regions are most movable as indicated by molecular dynamics (Ichiye, Olafson, Swamina & Karplus, 1986) and NMR (Smith, Sutcliffe, Redfield & Dobson, 1993) studies of HEL. The conformational flexibility of the substrate-binding region may be required to accommodate the substrate saccharide. When the NAG2 molecule is adopted in the cleft, the sugar molecule excludes the water molecules, some of which are hydrogen bonded to residues, Glu35, Gln57, Asn59, Trp63, Ala107, Val109, *etc.* (Harata, 1993). The two lobes of the cleft are so moved that these residues form hydrogen bonds with NAG2 and are found to be in favorable van der Waals contacts.

The NAG2 molecule is located parallel to the β-sheet comprising residues 42–55. The G1 and G2 pyranose rings are stacked with side-chain groups of Asn46 and Asp52. The inner side of the β-sheet forms a hydrophilic wall of the active-site cleft and a hydrogen-bond network is constructed with water molecules in the native crystal. Side-chain groups of Asn46, Asp48, Ser50 and Asp52 are linked by hydrogen bonds to form a planar hydrogen-bond network. In the NAG2 complex, the hydrophilic wall faces the hydrophobic pyranose rings. Hydrogen-bonding contacts among these four residues are reserved even in the presence of NAG2. However, the resulting low dielectric constant environment may increase the strength of the hydrogen bonds and electrostatic force (Quiocho, 1986). The face-to-face contact of the sugar ring with aromatic side-chain groups is frequently observed in the structures of sugar-bound proteins. The indole moiety of Trp62 in HEL is stacked with a pyranose ring of trisaccharides and the importance of the hydrophobic contact has been stressed (Ford *et al.*, 1974; Strynadka & James, 1991; Cheetham, Artymiuk & Phillips, 1992). On the other hand, in the TEL–NAG2 complex the pyranose rings of NAG2 face side-chain groups of Asn46, Thr47, Asp48 and Asp52 to stabilize the structure not only by van der Waals forces but also by electrostatic forces between H atoms of the pyranose ring and O atoms of side-chain groups. The conformational change observed in residues 46–49 is caused so that the side-chain groups can make better contacts with the pyranose rings of NAG2.

References

BERTHOU, J., LIFCHITZ, A., ARTYMIUK, P. J. & JOLLÉS, P. (1983). *Proc. R. Soc. London Ser. B*, **217**, 471–489.

BLAKE, C. C. F., JOHNSON, L. N., MAIR, G. A., NORTH, A. C. T., PHILLIPS, D. C. & SARMA, V. R. (1967). *Proc. R. Soc. London Ser. B*, **167**, 378–388.

BLAKE, C. C. F., KOENIG, D. F., MAIR, G. A., NORTH, A. C. T., PHILLIPS, D. C. & SARMA, V. R. (1965). *Nature (London)*, **206**, 757–763.

BRÜNGER, A. T., KURIYAN, J. & KARPLUS, M. (1987). *Science*, **235**, 458–460.

CHEETHAM, J. C., ARTYMIUK, P. J. & PHILLIPS, D. C. (1992). *J. Mol. Biol.* **224**, 613–628.

FORD, L. O., JOHNSON, L. N., MACHIN, P. A., PHILLIPS, D. C. & TJIAN, R. (1974). *J. Mol. Biol.* **88**, 349–371.

FRENCH, A. D. & MURPHY, V. G. (1973). *Carbohydr. Res.* **27**, 391–406.

HARATA, K. (1993). *Acta Cryst.* D**49**, 497–504.

ICHIYE, T., OLAFSON, B. D., SWAMINA, S. & KARPLUS, M. (1986). *Biopolymers*, **25**, 1909–1937.

IMOTO, T., JOHNSON, L. N., NORTH, A. C. T., PHILLIPS, D. C. & RUPLEY, J. A. (1972). *The Enzymes*, edited by P. D. BOYER, Vol. 7, pp. 665–868. London: Academic Press.

JOHNSON, L. N., CHEETHAM, J., MCLAUGHLIN, P. J., ACHARYA, K. R., BARFORD, D. & PHILLIPS, D. C. (1988). *Current Topics in Microbiology and Immunology*, Vol. 139, pp. 81–134. Berlin: Springer-Verlag.

KUNDROT, C. E. & RICHARDS, F. M. (1987). *J. Mol. Biol.* **193**, 157–170.

KURACHI, K., SIEKER, L. C. & JENSEN, L. H. (1976). *J. Mol. Biol.* **101**, 11–24.

LARUE, J. N. & SPECK, J. C. JR (1970). *J. Biol. Chem.* **245**, 1985–1991.

LUZZATI, V. (1952). *Acta Cryst.* **5**, 802–810.

MO, F. & JENSEN, L. H. (1978). *Acta Cryst.* B**34**, 1562–1569.

PERKINS, S. J., JOHNSON, L. N., MACHIN, P. A. & PHILLIPS, D. C. (1978). *Biochem. J.* **173**, 607–616.

QUIOCHO, F. A. (1986). *Annu. Rev. Biochem.* **5**, 287–315.

RAMANADHAM, M., SIEKER, L. C. & JENSEN, L. H. (1990). *Acta Cryst.* B**46**, 63–69.

RAO, S. T., HOGLE, J. & SUNDARALINGAM, M. (1983). *Acta Cryst.* C**39**, 237–240.

SMITH, L. J., SUTCLIFFE, M. J., REDFIELD, C. & DOBSON, C. M. (1993). *J. Mol. Biol.* **229**, 930–944.

STRYNADKA, N. C. J. & JAMES, M. N. G. (1991). *J. Mol. Biol.*, **220**, 401–424.